Analysis of Small-Angle X-ray Scattering Data for Model Polyurethane Ionomers: Evaluation of Hard-Sphere Models

Susan A. Visser and Stuart L. Cooper*

Department of Chemical Engineering, University of Wisconsin—Madison, Madison, Wisconsin 53706

Received August 10, 1990; Revised Manuscript Received November 6, 1990

ABSTRACT: The effect of pendant-anion type, polyol type, and polyol molecular weight on the morphology of model polyurethane ionomers was studied by small-angle X-ray scattering (SAXS). A liquidlike hard-sphere model and three new models of ionomer morphology were evaluated to determine their utility in analyzing ionomer SAXS data. Analysis of the SAXS data with a liquidlike hard-sphere model revealed that the carboxylated ionomers had lower degrees of phase separation, larger aggregate sizes, and lower aggregate number densities than their sulfonated analogues. Polyol type had a similar effect in sulfonated and carboxylated ionomers; morphological parameters depended on polyol polarity and chain cross section. Polyol molecular weight also affected carboxylated and sulfonated ionomers similarly. Evaluation of new models of ionomer morphology for analysis of SAXS data revealed that two of the three models were inadequate. The adhesive hard-sphere model and the local ordering model were capable of qualitatively reproducing the ionomer scattering patterns; however, neither model provided good quantitative agreement with the data with physically reasonable parameters. A liquidlike polydisperse hard sphere model gave excellent fits to the ionomer peak and high-q tails of the scattering data. Modeling of the sulfonated polyurethane ionomer systems with different polyol types revealed that inclusion of polydispersity effects in ionomer scattering analysis is vital; failure to consider polydispersity could allow deduction of erroneous morphological parameters from SAXS data.

Introduction

The precise morphological nature of many ionomers is still an open question. While it is widely accepted that the ionic groups aggregate in the bulk, forming physical cross-links that impart dramatic changes in material properties,[1-7] the structure of the aggregates and their arrangement in the polymer matrix are unclear.[2,8] Early in the study of ionomers, Eisenberg proposed the so-called multiplet-cluster model of ionomer morphology.[9] The ionic groups are postulated to exist in two distinct environments, multiplets and clusters. Multiplets are groups of a few ion pairs (no more than eight) that are tightly aggregated and exclude all nonionic material. Geometric constraints limit their size to 0.6-nm spherical diameter.[9] Clusters are collections of several multiplets that form a domain locally rich in ionic material but containing a significant fraction of nonionic material as well. Clusters are envisioned to be on the order of 5–10 nm in diameter. Both spectroscopic and thermal analysis experiments have produced evidence consistent with the multiplet–cluster model.[7,10-12]

Recently, Eisenberg et al.[13] proposed a new model for ionomer morphology that reconciles many of the previously unexplained features seen in the mechanical properties of ionomers. The model envisions the basic unit of ionic aggregation as multiplets, as before. However, in this model, the regions of restricted mobility surrounding the multiplets begin to overlap as the ionic content becomes large, creating ion-rich and ion-poor phases. The ion-rich phases are again termed clusters. The phase separation gives rise to some of the unusual features of ionomers, including the appearance of the "ionic transition" at high temperatures in dynamic mechanical studies. The qualitative agreement of this model with available experiment evidence is convincing.

The study of ionomer morphology is most often pursued by using small-angle X-ray scattering (SAXS). The typical ionomer SAXS pattern shows evidence of ionic aggregation with the presence of a broad peak centered at q values of 0.5–5 nm^{-1}, where $q = (4\pi/\lambda) \sin \theta$. 2θ is the scattering angle, and λ is the X-ray wavelength. The so-called "ionomer peak" is usually accompanied by a sharp upturn in intensity at low q values. Anomalous SAXS analysis of ionomers has proven that ionic material gives rise to the upturn in intensity[14,15] and has led to the hypothesis that the upturn results from an inhomogeneous distribution of ionic groups in the polymer matrix. An additional feature is sometimes seen in SAXS patterns of semicrystalline ionomers; a peak at a q value lower than that of the ionomer peak may arise from scattering from the crystalline lamallae.[16]

Various microstructural models have been proposed to quantitatively explain the observed SAXS patterns. The models can be broadly divided into two groups, the intraparticle interference models[17-19] and the interparticle interference models.[8,20-21] The intraparticle interference models attribute the ionomer peak to scattering arising from short-range order within the ionic aggregates. Quantitative evaluation of the intraparticle interference models indicated poor agreement between model and experiment, however.[8] In contrast, experimental evidence in support of the interparticle interference models continues to accumulate.[8,22-24] The interparticle interference models postulate that the ionic aggregates are arranged in the polymer matrix with some degree of order; the ionomer peak arises from scattering between ionic aggregates.

A moderately successful interparticle interference model for quantitative evaluation of ionomer SAXS data was proposed by Yarusso and Cooper.[8] Their liquidlike model assumes that the ionic aggregates are hard spheres of radius R, distributed with a liquidlike degree of order in the polymer matrix. The ionic aggregates are surrounded by an impenetrable sheath of polymer to give a radius of closest approach $D/2 > R$. The polymer sheath arises from the connectivity of the polymer chains to the ionic groups. The existence of a polymer sheath has been demonstrated for block copolymers possessing a liquidlike spherical morphology[23,24] and, indirectly, for sulfonated polyurethane ionomers by small-angle neutron scattering.[25] The Yarusso model is consistent with the

0024-9297/91/2224-2584$02.50/0

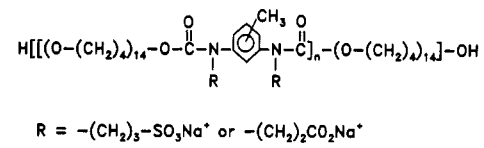

R = $-(CH_2)_3-SO_3Na^+$ or $-(CH_2)_2CO_2Na^+$

Figure 1. Structure of the model polyurethane ionomer, using a 1000 molecular weight PTMO polyol as an example. n is the overall degree of polymerization.

new generalized model of ionomer morphology proposed by Eisenberg et al.[13] While highly successful in modeling the ionomer peak,[26,27] the liquidlike hard-sphere model fails to reproduce the upturn in intensity at low q.

Several modifications to current interparticle interference models are investigated in this paper. Furthermore, having shown a strong dependence of ionomer properties on pendant-anion type in the previous paper,[28] we concentrate in this paper on the morphological analysis of a series of carboxylated and sulfonated model polyurethane ionomers. Hashimoto et al. performed a similar comparison of carboxylated and sulfonated perfluorinated ionomer membranes using X-ray scattering;[16] it was observed that sulfonated ionomers had larger ionic clusters and lower degrees of crystallinity than carboxylated ionomers. A study of sulfonated and carboxylated polystyrene ionomers revealed essentially identical cluster sizes for the two types of ionomers.[26] In the physical property characterization of the model polyurethane ionomers,[28] the carboxylated ionomers had higher than expected Young's moduli and, in dynamic mechanical analysis experiments, higher cross-linking efficiencies than sulfonated ionomers. Correlations between these unusual properties and the morphology of the carboxylated and sulfonated ionomers are demonstrated here. In addition, the effect of polyol type and polyol molecular weight are investigated in the model ionomer systems.

Experimental Setup

Sample Preparation. The synthesis of the model polyurethane ionomers was described in the previous paper.[28] The model polyurethane ionomers are 1:1 copolymers of a polyol and tolylene diisocyanate (TDI), which have sodium propylsulfonate or sodium ethylcarboxylate groups grafted solely at the urethane linkages. A typical model polyurethane ionomer chemical structure is shown in Figure 1. Three polyol types were investigated: poly(tetramethylene oxide) (PTMO, M_n = 990, 2070), poly(propylene oxide) (PPO, average molecular weight 1000, 2000), and poly(ethylene oxide) (PEO, average molecular weight 1000).

Ionomer samples for SAXS were examined as solution-cast films. The sulfonated ionomers were cast at 60 °C from *N,N*-dimethylacetamide. The carboxylated ionomers were cast at 25 °C from 4:1 v/v toluene/methanol, except for the 98% carboxylated PTMO(1000)/TDI ionomers and the carboxylated PEO(1000)/TDI ionomers, because of solubility constraints. (The parenthetical 1000 indicates the approximate molecular weight of the polyol.) The 98% carboxylated PTMO(1000)/TDI ionomer was cast from a 2:1 v/v toluene/methanol solution. The carboxylated PEO(1000)/TDI ionomer was cast from methanol. Films were dried in a 50 °C vacuum oven for at least 1 week before use to remove residual solvent and water.

SAXS Measurements. The small-angle X-ray scattering (SAXS) data were obtained by using an Elliot GX-21 rotating-anode generator, an Anton-Paar compact Kratky scattering camera, and a TEC Model 211 linear position-sensitive detector. Cu Kα radiation was monochromatized by using a nickel filter and pulse height discrimination. The scattering camera has a sample-to-detector distance of 60 cm and a detector length of approximately 8 cm. This configuration allowed a q ($q = (4\pi/\lambda)/\sin\theta$, where 2θ is the scattering angle and λ is the wavelength of the radiation) range of 5.7 nm^{-1}, with a minimum q of 0.15 nm^{-1} due to the position of the beam stop, to be probed. The detector length was divided into 128 channels for a resolution of $\simeq$0.05 nm^{-1}. All data were collected at room temperature.

The data were corrected for detector sensitivity, parasitic and background scattering, and absorption of X-rays by the sample. The beam profile along the slit length was measured, and the iterative method developed by Lake[29] was used to desmear the data. Absolute intensities expressed in terms of I/I_eV, where I_e is the intensity scattered by a single electron and V is the scattering volume, were determined by comparing the sample scattering intensity to that from a calibrated Lupolen (polyethylene) standard.[30] Background scattering was determined by a fitting of the SAXS data in the high-q region using Porod's law[31] plus a constant background term.

Sample Nomenclature. Samples are designated with the first letter indicating the polyol type (M = PTMO, P = PPO, E = PEO), the number indicating the polyol molecular weight in thousands, the letter describing the pendant ionic-group type (S = sulfonate, C = carboxylate), and the final two letters the chemical symbol for the neutralizing cation. Thus, M1SNa indicates a 1:1 copolymer of PTMO, molecular weight 1000, and TDI, sulfonated and neutralized with sodium.

Results and Discussion

The SAXS data presented here show some or all of the features commonly found in ionomer SAXS patterns: a peak at 0.6–2 nm^{-1} in q, an upturn in intensity at low q, and, in the case of E1CNa, a low-q peak, probably arising from scattering from crystalline lamallae in the sample. Similar low-q features arising from sample crystallinity have been observed in a number of semicrystalline ionomers.[26,32-36] Only the SAXS pattern of P1CNa fails to exhibit an ionomer peak (or a shoulder on the upturn); this indicates the absence of ionic aggregation.

For the initial, detailed analysis of the SAXS data, a modified version of the liquidlike hard-sphere Yarusso model[8] was used. The spherical aggregates of radius R have an electron density of ρ_1, and the electron density of the sheath of radius $D/2$ and the polymer matrix is ρ_0. Originally, Yarusso and Cooper[26] used the Fournet three-body interference function,[37] based on the Born–Green theory of liquid structure. However, as Ding et al. noted,[27] Kinning and Thomas[38] have since shown that the Percus–Yevick total correlation function,[39] as solved by Wertheim[40] and Theile[41], provides a more satisfactory fit to scattering data from diblock copolymers with a spherical morphology. Furthermore, the Percus–Yevick approximation has been shown to agree well with Monte Carlo simulations for scattering from both nonadhesive[42] and adhesive[43] hard spheres over a wide range of conditions. The Percus–Yevick equation is expected to give better results for high ionic aggregate concentrations, where many-body interactions become more important.

The equation describing the scattered intensity from this model is

$$\frac{I}{I_eV} = \frac{1}{v_p}\left[\frac{4\pi R^3}{3}\right]^2(\rho_1 - \rho_0)^2\Phi^2(qR)S(qD) \qquad (1)$$

where I_e is the scattering from a single electron, V is the scattering volume, v_p is the volume of material per ionic aggregate (the inverse of the aggregate number density), and Φ is the scattering from a single sphere:[44]

$$\Phi(qR) = \frac{3}{(qR)^3}[\sin(qR) - (qR)\cos(qR)] \qquad (2)$$

$S(q)$ is the interference function, or structure factor, which has been given in the Percus–Yevick form previously.[27]

The modeling results are presented in Table I and are discussed as the data are presented below. η is the volume fraction of hard spheres. Note that for ionomers whose ionic peaks were merged with the upturn, the shoulders

Table I
Model-Fit Parameters for Yarusso Model

sample	% subst[a]	R, nm	D, nm	v_p, nm^3	$\rho_1 - \rho_0$, nm^{-3}	$g^{b,c}$	ρ_1,[c] nm^{-3}
M1SNa	93	1.46	4.60	178	264	0.073	591
M1CNa	98	1.70	5.88	842	261	0.024	588
M1CNa	57	1.19	4.00	199	268	0.036	595
M2SNa	94	1.59	5.52	332	222	0.012	549
M2CNa	59	1.47	5.52	1362	342	0.010	669
P1SNa	95	1.11	4.42	77	319	0.074	654
P1CNa	89						
P2SNa	93	1.38	5.44	164	209	0.067	544
P2CNa	96	1.73	4.80	281	127	0.077	462
E1SNa	100	1.14	4.00	123	212	0.051	589
E1CNa[d]	96	1.22	4.42	219	201	0.035	578

[a] From elemental analysis[28] for sulfur, in the case of sulfonated ionomers, or for sodium, for carboxylated ionomers. [b] $g = 4\pi R^3/3v_p$, volume fraction ionic aggregates. [c] Calculated from model parameters (see text). [d] Fit of high-q peak.

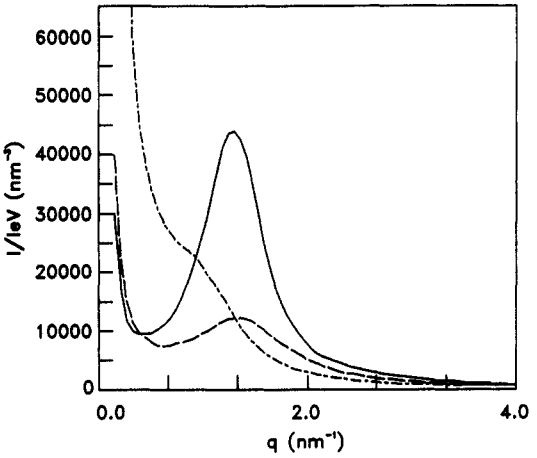

Figure 2. Small-angle X-ray scattering patterns for sulfonated and carboxylated ionomers based on 1000 molecular weight PTMO: (—) M1SNa, (- - -), M1CNa (98% carboxylated), (– –) M1CNa (57% carboxylated).

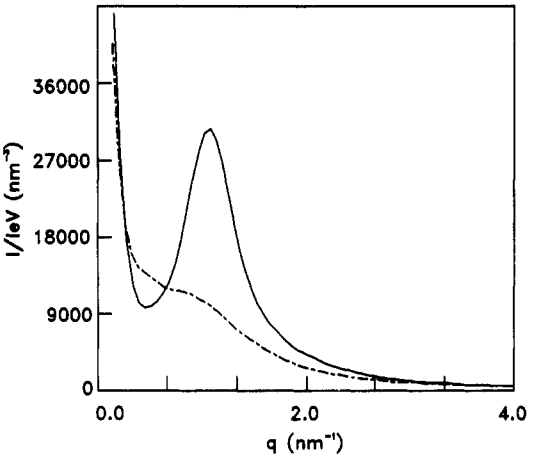

Figure 3. Small-angle X-ray scattering patterns for sulfonated and carboxylated ionomers based on 2000 molecular weight PTMO: (—) M2SNa, (- - -) M2CNa.

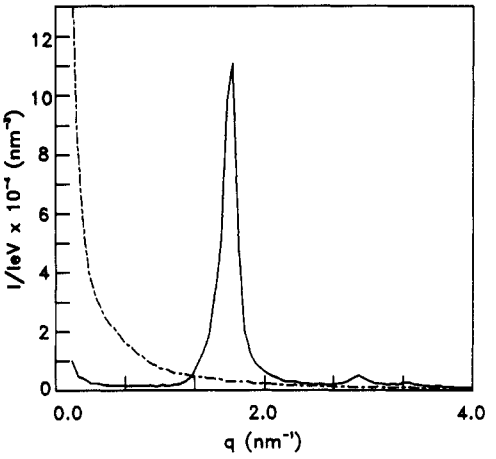

Figure 4. Small-angle X-ray scattering patterns for sulfonated and carboxylated ionomers based on 1000 molecular weight PPO: (—) P1SNa, (- - -) P1CNa.

on the upturn were modeled as peaks in the Yarusso model as a basis for comparison only. The uncertainty surrounding deconvolution of the upturn and the ionic shoulder prevents more accurate analysis of the morphology of these two ionomers, M1CNa (98% carboxylated) and M2CNa (59% carboxylated). The R values presented for these two ionomers, however, are consistent with those that could be extracted by a simple Bragg's law analysis and are, thus, sufficient for the comparison offered here.

Effect of Pendant-Anion Type. The effect of pendant-anion type on the morphology of model polyurethane ionomers is addressed in this section. The regular placement of ionic groups at the urethane linkages of these ionomers, as well as the essentially identical chain architecture of the carboxylated and sulfonated ionomer pairs, makes the model polyurethane an excellent system for studying the influence of pendant-anion type. This section also addresses three questions that arose in the physical property characterization of the model polyurethane ionomers: Why are the Young's moduli of the carboxylated ionomers nearly as high as their sulfonated analogues, despite the lower acid strength and presumably lower crosslink cohesiveness of the carboxylate groups? Why does P1CNa have lower tensile properties (e.g., σ_b, ϵ_b) than the lower ion content P2CNa? Why is the Young's modulus of P2CNa greater than those of P1CNa and P2SNa?

The SAXS patterns for the carboxylated and sulfonated ionomers are shown in Figures 2–6. In all cases, the q value at which the maximum is attained, q^*, is greater for the sulfonated ionomer than for its carboxylated analogue. Since an interparticle interference model is postulated, this implies that the average spacing between the ionic aggregates is greater in the carboxylated than in the sulfonated ionomers, which is reflected in the v_p values in Table I. The degree of phase separation in the ionomers can be assessed from the v_p values and the interaggregate spacings. A lower degree of phase separation necessitates a greater number of ionic groups dispersed in the polymer matrix, lowering the aggregate number density and increasing interaggregate spacing. Both the aggregate number densities ($1/v_p$) and the interaggregate spacings indicate higher degrees of phase separation in the sulfonated than in the carboxylated ionomers, as was observed in the differential scanning calorimetry (DSC) and dynamic mechanical thermal analysis (DMTA) results of

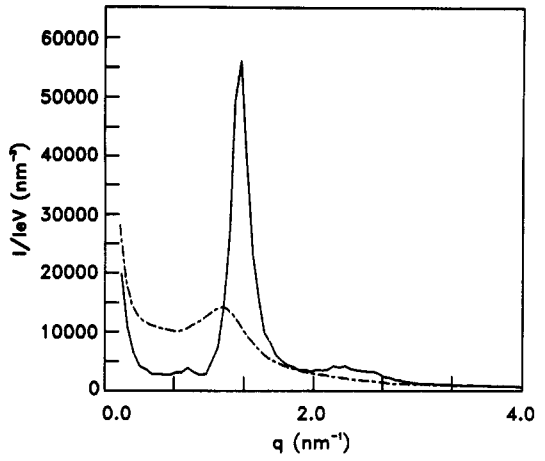

Figure 5. Small-angle X-ray scattering patterns for sulfonated and carboxylated ionomers based on 2000 molecular weight PPO: (—) P2SNa, (- - -) P2CNa.

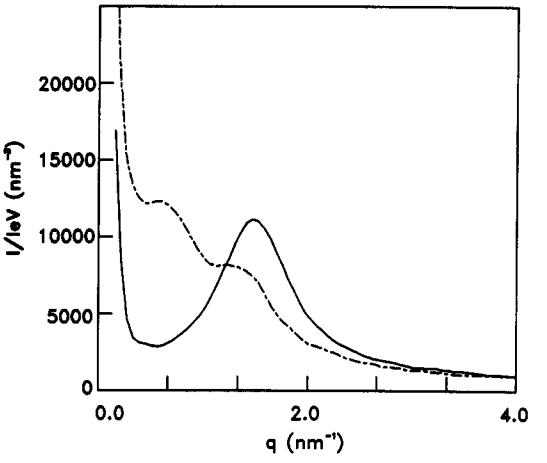

Figure 6. Small-angle X-ray scattering patterns for sulfonated and carboxylated ionomers based on 1000 molecular weight PEO: (—) E1SNa, (- - -) E1CNa.

the previous paper.[28] Differences in phase separation are also reflected in the volume fractions of ionic aggregates, g, which are less for the carboxylated than for the sulfonated ionomers based on 1000 molecular weight polyols. The g values for the analogous (identical polyol type and polyol molecular weight) carboxylated and sulfonated ionomer pairs based on 2000 molecular weight polyols (M2SNa vs M2CNa; P2SNa vs P2CNa) are similar, indicating similar degrees of phase separation. Again, this corresponds to the trends seen in the DSC and DMTA results of the previous paper.[28]

The size of the ionic aggregates (R) are generally greater for the carboxylated ionomers that for their sulfonated analogues. The larger aggregate sizes in the carboxylated ionomers are probably indicative of a larger number of ionic groups in their ionic aggregates. The higher physical cross-link functionality explains the high Young's moduli of the carboxylated ionomers despite the relative weakness of the individual carboxylate groups as cross-link points.

While differences in casting solvents for sulfonated and carboxylated ionomers may have caused some of the observed differences in R values, a previous study[27] of the effect of casting solvent on ionic aggregate size of M1SNa ionomers showed a maximum change in R of only 0.06 nm as casting solvent was varied from *N,N*-dimethylformamide to 5:1 tetrahydrofuran/water to compression molding (equivalent to casting from PTMO). Thus, while changes in casting solvent will have some effect on R values, the R values used here for comparison are expected to be dominated by anion effects and not by casting solvent effects.

For M2SNa and M2CNa, the R values are similar; however, the increased v_p value for M2CNa suggests an increase in the number of ionic groups dissolved in the matrix.[8,45] Since larger dipole–dipole interactions are expected between sulfonate groups, leading to a larger driving force for ionic aggregation,[16] it seems logical that the $1/v_p$ (aggregate number density) values are larger for the sulfonated than the carboxylated ionomers. A similar situation is seen for the E1SNa and E1CNa ionomers.

The absence of an ionomer peak in the P1CNa SAXS pattern indicates that little or no ionic aggregation is occurring, leading to the poor tensile properties of P1CNa.[28] The large size (R) and high ionic aggregate volume fraction (g) in P2CNa compared to P2SNa or P1SNa account for the high Young's modulus of P2CNa.

The electron density differences for the carboxylated versus the sulfonated ionomers follow no clear trends. While accurate estimates of matrix electron densities are difficult to compute, if the matrices are assumed to consist predominantly of the soft-segment polyols, some estimates can be calculated. With density values of 0.98 g/cm^3 for PTMO (for amorphous PTMO soft segments in segmented polyether–polyesters[46]), 1.01 g/cm^3 for PPO (for 2000 molecular weight oligomer, no ethylene oxide capping[47]), and 1.13 g/cm^3 for PEO,[48] matrix electron densities of 327 e/nm^3 for PTMO, 335 e/nm^3 for PPO, and 377 e/nm^3 for PEO can be calculated. In combination with the electron density difference ($\rho_1 - \rho_0$) values obtained from the Yarusso model, the aggregate electron densities ρ_1 shown in Table I are derived. The aggregate electron densities of M1SNa, M1CNa, E1SNa, and E1CNa are similar, reflecting similar packing densities in the ionic aggregates. The ρ_1 value of M2SNa is less than the ρ_1 value for M2CNa, perhaps reflecting that the cations are less densely packed within the more numerous aggregates in M2SNa. In contrast, the ρ_1 value for P2SNa is greater than that of P2CNa, implying the opposite trend in the effect of pendant-anion type on cation packing density.

Effect of Polyol Type. The effect of polyol type can be seen most clearly in the ionomers based on 1000 molecular weight polyols. Comparing the sulfonated ionomers, the q^* values decrease in the order P1SNa > E1SNa > M1SNa. Interparticle interference as the source of scattering indicates an increase in the average spacing between aggregates in the order M1SNa > E1SNa > P1SNa, as reflected in the v_p values in Table I. The results suggest that the aggregate number densities in the sulfonated ionomers decrease in the order P1SNa > E1SNa > M1SNa. The R values also indicate that M1SNa has larger ionic aggregates than P1SNa or E1SNa; the aggregate sizes of E1SNa and P1SNa are similar.

The high polarity of the PEO polyol and low ionic aggregate volume fraction in E1SNa compared to P1SNa and M1SNa probably account for the smaller ionic aggregate size in E1SNa. For P1SNa and M1SNa, it is possible that the larger cross section of the PPO chain results in the smaller domain sizes. As all ionic groups are closely attached to the polymer chains, the more bulky PPO polymer chains will limit the number of ionic groups that can aggregate within a distance close enough for Coulombic attractions to dominate. The maximum size of the ionic domains will be related to the specific volume of the polyol chain monomer compared to that of the ionic pair, causing PPO-based ionomers to have smaller ionic domains than PTMO-based ionomers. A similar explanation has been advanced to account for differences

observed in ionic domain sizes of telechelic ionomers.[22]

The most striking difference between P1SNa, E1SNa, and M1SNa is seen directly in the SAXS patterns. E1SNa and M1SNa each exhibit a single broad ionomer peak, indicating relatively disordered structures. In contrast, the regular spacing of the ionic aggregates in P1SNa is reflected in the sharpness of its ionomer peak. Furthermore, P1SNa exhibits not only a first-order ionomer peak but also three higher order scattering peaks. The ratio of q values at which the peaks appear for P1SNa is 1:1.7:1.98:2.17. If it is assumed that symmetry constraints or the width of the first-order peak cause the absence of a noticable second-order scattering peak, the peak ratios for P1SNa are in close agreement with the ratios expected for either a simple cubic or a body-centered cubic lattice of spherical particles (1:1.41:1.73:2.00:2.24). While not a typical morphology for ionomer systems, highly ordered structures have also been noted in telechelic ionomers,[49,50] ionenes,[51] and ion-containing block copolymers.[52]

The highly ordered arrangement of the ionic aggregates in P1SNa exceeds the ordering assumptions inherent in the Yarusso model, yet the model still gives an accurate description of the ionomer morphology. In particular, the Yarusso model parameters reflect the regular structure of P1SNa; the average distance between particles, $v_p^{1/3}$, is approximately equal to the closest approach distance D (4.3 vs 4.4 nm). The range of ionomer morphologies that can be described by using the Yarusso model is apparently greater than previously considered.

Comparison of E1CNa and M1CNa show similar trends in the effect of polyol type as are seen in the sulfonated ionomers. Substantially smaller values of v_p and R are found for E1CNa than for M1CNa, suggesting that the PEO-based material has more numerous, but smaller, ionic aggregates.

The aggregate electron densities ρ_1 calculated for M1SNa, M1CNa, E1SNa, and E1CNa are similar, indicating similar cation packing densities in the ionic aggregates. In contrast, the ρ_1 value calculated for P1SNa is substantially higher, suggesting higher cation packing densities. This may also be a reflection of the greater number of ionic groups present in the ionic aggregates than dispersed in the polymer matrix.

The upturn in intensity at low q and evidence of ionic aggregation in the form of the ionomer peak are seen for all ionomers based on 2000 molecular weight polyols. Comparing M2SNa and P2SNa, the PPO-based ionomer again has smaller (R) and more numerous ($1/v_p$) ionic aggregates than the PTMO-based ionomer. The regular morphology of P2SNa compared to M2SNa is seen in the sharpness of the ionomer peak in P2SNa, in the presence of a second-order scattering peak in the P2SNa scattering pattern (this peak was fit along with the first-order peak in the modeling analysis), and in the similarity between the average distance between particles ($v_p^{1/3}$) and the closest approach distance (D) for P2SNa (5.5 vs 5.4 nm).

M2CNa and P2CNa can also be compared with the admonition that the ionic contents of the polymers are not the same. The degree of substitution at the urethane nitrogen is 59% for M2CNa but 96% for P2CNa. With that caveat, it should not seem too surprising that the R value for P2CNa is greater than that for M2CNa. Comparing the R values in Table I of the 57% and 98% substituted M1CNa ionomers, it is seen that increasing the degree of substitution increases the R values. Thus, the lower R values for M2CNa compared to P2CNa probably result from the degree of ionic substitution. If the degrees of carboxylation were identical for the two polymers, the R values would probably decrease in the order M2CNa > P2CNa, as seen above for the other PTMO- and PPO-based model polyurethane ionomers.

Finally, comparisons may also be made of aggregate electron densities ρ_1 for the ionomers based on 2000 molecular weight polyols. The ρ_1 values of P2SNa and M2SNa are similar, suggesting approximately equivalent cation packing densities in the aggregates. The ρ_1 value for M2CNa is greater than that of P2CNa; the cation packing is apparently less dense in P2CNa.

Effect of Polyol Molecular Weight. SAXS curves for the PTMO-based ionomers are shown in Figures 2 and 3. As polyol molecular weight increases, the peak moves to lower q, and v_p increases, regardless of pendant-anion type, as expected. Increasing polyol molecular weight induces increased spacing between aggregates. The R values increase with polyol molecular weight for the sulfonated ionomers, as was observed by Ding et al.,[27] but the R values of the carboxylated ionomers decrease with polyol molecular weight. The trend for the carboxylated ionomers is probably more a reflection of the degree of ionic substitution, as discussed above, however.

Comparisons of P1SNa and P2SNa, whose SAXS patterns appear in Figures 4 and 5, indicate trends in R and v_p similar to those seen for M1SNa and M2SNa. R and v_p increase with polyol molecular weight. The effect of polyol molecular weight is most dramatic in the carboxylated PPO-based ionomers, where P2CNa displays evidence of ionic aggregation (the ionomer peak) while P1CNa does not.

Evaluation of Modified Interparticle Interference Models To Describe Ionomer SAXS Data. Liquidlike Polydisperse Hard-Sphere Model. To this point, it has been assumed that the ionic aggregates are spherical and monodisperse. Direct observation of ionic aggregates by high-voltage transmission electron microscopy (HVEM) has confirmed their spherical shape in sulfonated polystyrene ionomers;[53] however, the same study demonstrated a significant degree of polydispersity in aggregate size. Furthermore, introducing a degree of polydispersity into the modeling analysis would help smooth out the high-q oscillations resulting from the hard-sphere assumption in the model presented above, thereby producing better agreement between model and experimental data at high q.

An expression for the interference function for polydisperse hard spheres has been derived by Vrij[54] and has been applied by Kinning et al. to the analysis of block copolymer SAXS data.[24] Vrij's equations, adapted for SAXS and the liquidlike model, are[55]

$$Q_k = \frac{4\pi(\Delta\rho)}{q^3}[\sin(qR_k) - (qR_k)\cos(qR_k)] \tag{3}$$

$$X_k = qD_k/2 \tag{4}$$

$$\Phi_k = (3/X_k^3)[\sin X_k - X_k \cos X_k] \tag{5}$$

$$\Psi_k = X_k^{-1} \sin X_k \tag{6}$$

$$\langle \Xi \rangle = (\pi/6)\sum_{k=1}^{P} p_k \Xi_k \tag{7}$$

$$(-\pi/6)(1-\xi_3)^4\Omega(q) = \langle Q^2\rangle T_1T_1^* + \langle D^6\Phi^2\rangle T_2T_2^* + 9\langle D^4\Psi^2\rangle T_3T_3^* + \langle D^3\Phi Q\rangle (T_1T_2^* + T_1^*T_2) + 3\langle D^2\Psi Q\rangle (T_1T_3^* + T_1^*T_3) + 3\langle D^5\Phi\Psi\rangle (T_2T_3^* + T_2^*T_3) \tag{8}$$

where

$$T_1 = F_{11}F_{22} - F_{12}F_{21} \quad (9)$$

$$T_2 = F_{21}\langle DQe^{iX}\rangle - F_{22}\langle Qe^{iX}\rangle \quad (10)$$

$$T_3 = F_{12}\langle Qe^{iX}\rangle - F_{11}\langle DQe^{iX}\rangle \quad (11)$$

$$F_{11} = 1 - \langle D^3\rangle + \langle D^3\Phi e^{iX}\rangle \quad (12)$$

$$F_{12} = \langle D^4\Phi e^{iX}\rangle \quad (13)$$

$$F_{22} = 1 - \langle D^3\rangle + 3\langle D^3\Psi e^{iX}\rangle \quad (14)$$

$$F_{21} = [1 - \langle D^3\rangle]\frac{iq}{2} - 3\langle D^2\rangle + \langle D^2\Psi e^{iX}\rangle \quad (15)$$

$$\Gamma(q) = [1 - \langle D^3\rangle]^{-4}T_1T_1^* \quad (16)$$

$$I/I_eV = -\Omega(q)/\Gamma(q) \quad (17)$$

In these equations, k is the counting index of an assembly of hard spheres having P distinct diameters, i is the imaginary unit, and an asterisk denotes the complex conjugate. p_k is the number density of spheres of that diameter, equal to r_k/v_p, if r_k is the probability density in a normalized distribution of diameters. Equation 7 simply explains the averaging process described by angular brackets; Ξ can represent D^n, Q, Φ, Ψ, e^{iX}, or any combination of these functions. For numerical evaluation, the distribution was taken to be Gaussian in D with a fractional standard deviation $\sigma_f = \sigma_D/\bar{D}$, and $\pm 3\sigma_f$ were covered in 39 slices. The mean values will be denoted by $\bar{D}$ and $\bar{R}$. Note that the fractional deviation in R was assumed to equal that in D, so that all aggregates have $R_k/D_k = \bar{R}/\bar{D}$.

The model fit parameters for this model are presented in Table II. Only the data from the sulfonated ionomers were modeled because of the ambiguities inherent in modeling the shoulders in the carboxylated ionomer data. Comparing the model fit parameters in Tables I and II, there is little change in R, D, or v_p for the PTMO- and PPO-based ionomers for the two cases. Also, the fractional standard deviation of the Gaussian size distribution σ_f is relatively small but noticeable for these polymers. The dramatic improvement in the fit of the model to the high-q data obtained by introducing this small degree of polydispersity, however, is illustrated in Figure 7. The high-q oscillations in the model fit of the monodisperse hard-sphere model are smoothed out by the introduction of polydispersity, providing a much more satisfactory fit to the peak and tail region of the data. Similar improvements in the high-q fits were observed for the other sulfonated ionomers (not shown).

The greatly changed R, D, and v_p values obtained by the polydisperse hard-sphere modeling of the E1SNa data compared to the parameters obtained by the monodisperse model illustrate the importance of including polydispersity considerations in modeling the SAXS data of ionomers. For highly polydisperse aggregate sizes, use of the monodisperse model can give misleading results. The σ_f value obtained for E1SNa indicates a substantial degree of polydispersity in aggregate size, a parameter clearly dependent on polyol type for the model polyurethane ionomers.

The introduction of another modeling parameter, σ_f, which cannot be determined independently, is a significant drawback to use of the polydisperse Percus–Yevick approximation. The modeling results for the PTMO- and PPO-based sulfonated polyurethane ionomers indicate that, for many ionomers, little information regarding aggregate size or arrangement would be lost by using the monodisperse Percus–Yevick approximation. A similar conclusion was reached by Register for modeling of sulfonated polystyrene SAXS data.[55] However, the improvement in the fit of the high-q data, as well as the significant changes in model parameters for E1SNa upon the introduction of polydispersity, suggest that ignoring polydispersity of aggregate sizes could lead to misleading interpretations of SAXS data in some ionomer systems. To obtain more precise knowledge of ionomer morphology using the liquidlike hard-sphere model, the polydisperse Percus–Yevick approximation is preferred.

Table II
Model-Fit Parameters for Liquidlike Polydisperse Hard-Sphere Model

sample	$\bar{R}$, nm	$\bar{D}$, nm	v_p, nm^3	σ_f	$\Delta\rho$, nm^{-3}
M1SNa	1.50	4.46	169	0.051	247
M2SNa	1.46	5.50	332	0.120	254
P1SNa	1.23	4.70	76	0.109	240
P2SNa	1.38	5.44	164	0.018	208
E1SNa	0.84	3.22	62	0.343	218

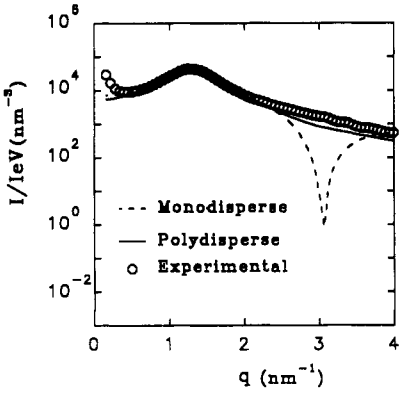

Figure 7. Comparison of monodisperse and polydisperse Percus–Yevick approximations within the Yarusso model to experimental data for M1SNa sample.

Adhesive Hard-Sphere Model. A major shortcoming of the liquidlike hard-sphere model in reproducing ionomer SAXS patterns is its inability to even qualitatively reproduce the upturn in intensity at low q. While both core-shell[17,19] and paracrystalline lattice[21] models can qualitatively fit both the ionomer peak and the upturn, Yarusso has shown that their quantitative fit to ionomer scattering data is poor.[8] Another source that could give rise to the upturn is a nonrandom distribution of ionic aggregates in the polymer matrix.

A number of investigators have suggested that an inhomogeneous distribution of aggregates gives rise to the upturn.[14,15,22,56] In the adhesive hard-sphere model proposed by Register,[55] it was postulated that large-scale fluctuations in the aggregate number density arise from attractions between the aggregates when the matrix is fluid, as the aggregates are high-order multipoles and presumably highly polarizable. Aggregation of ionic groups in the melt[2] and in solution[57] is a well-documented phenomenon. In the bulk, three situations were envisioned that could give rise to the inhomogeneous distribution of ionic groups.[55] The nonrandom distribution is frozen in if the glass transition of the material is greater than the observation temperature. This is probably the case for polystyrene ionomers. The inhomogeneous distribution of ionic aggregates could also result from the connectivity of the ionic groups and the polymer chains; entanglements and other topological constraints could prevent the aggregates from achieving a uniform distribution in the bulk. The influence of topological constraints on the physical properties of model polyurethane ionomers has been noted.[28] Finally,

Table III
Model-Fit Parameters for Adhesive Hard-Sphere Model

sample	R, nm	D, nm	η	$\Delta\rho$, nm^{-3}	λ	τ^a
M1SNa	1.29	5.62	0.0185	1702	135	0.197
M2SNa	1.44	6.80	0.0502	839	38.1	0.136
P1SNa	1.28	4.86	0.6481	257	12.1	−0.305
P2SNa	1.38	6.13	0.6164	223	8.80	−0.145

[a] τ is not a model-fit parameter but was calculated from model parameters.

the nonequilibrium morphology imposed by sample preparation conditions could result in a nonuniform distribution of aggregates. If the first mechanism is dominant or if the inhomogeneous distribution imposed by the second two has a form similar to that resulting from the first, an adhesive hard-sphere model could be used to describe the full ionomer SAXS curves.

There is only one adhesive hard-sphere potential function, $U(r)$, that has resulted in a closed-form expression for the interference function $S(qD)$ in the Percus–Yevick approximation. This is the adhesive hard-sphere model proposed by Baxter:[58]

$$\begin{aligned} U/kT &= \infty \quad 0 < r < D' \\ &= \ln [12\tau(D - D')/D] \quad D' < r < D \\ &= 0 \quad r > D \end{aligned} \tag{18}$$

where r is the center-to-center separation of the spheres, D is the diameter of the spheres, and $D - D'$ is a vanishingly small quantity. Regnaut and Ravey[59,60] presented an analytical expression for $S(q)$ based on the Baxter potential that can be represented as

$$S(q)^{-1} = [1 - \eta\tilde{c}(q)/v_h] \tag{19}$$

where $\tilde{c}(q)$ is the Fourier transform of the direct correlation function:

$$\frac{\tilde{c}(q)}{v_h} = -24\alpha\left[\frac{J_1(qD)}{qD}\right] - 24\beta\left[\frac{J_2(qD)}{qD}\right] - 12\eta\alpha\left[\frac{J_4(qD)}{qD}\right] - 2\eta\lambda^2\left[\frac{J_0(qD)}{qD}\right] + 2\lambda\left[\frac{\sin(qD)}{qD}\right] \tag{20}$$

$$J_n(qD) = \int_0^1 x^n \sin(qDx)\, dx \tag{21}$$

$$\alpha = (1 + 2\eta - \mu)^2/(1 - \eta)^2 \tag{22}$$

$$\beta = \frac{-3\eta(2 + \eta)^2 + 2\mu(1 + 7\eta + \eta^2) - \mu^2(2 + \eta)}{2(1 - \eta)^4} \tag{23}$$

$$\mu = \lambda\eta(1 - \eta) \tag{24}$$

and λ is a parameter representing the strength of the adhesion, related to τ by

$$\tau = \frac{(2 + \eta)}{2\lambda(1 - \eta)^2} - \frac{\eta}{1 - \eta} + \frac{\eta\lambda}{12} \tag{25}$$

where the lesser root for λ is taken.

The model was fit to the data for the sulfonated polyurethane ionomers, resulting in the best-fit parameters listed in Table III. The results, shown in Figures 8–10, indicate some discrepancies in quantitative reproduction of the data. For M2SNa, the model gives a relatively good fit to the upturn and the peak region, underestimating the extent of the upturn slightly; however, a high-q shoulder is predicted by the model that is not present in the data. A similar quality of fit is seen for the M1SNa sample (not shown), where the peak and upturn are well fit but a high-q shoulder appears in the model that is absent in the data. The model fit for P2SNa, shown in Figure 9, again gives a good fit to the upturn and peak regions, but a second maximum at $q \sim 2.3$ nm^{-1} is overpredicted by the model. The problems of a shoulder on the ionomer peak or an overprediction of the second maximum in q are absent in the model fit for P1SNa data, shown in Figure 10; however, the model fails to predict the slight upturn in intensity at low q.

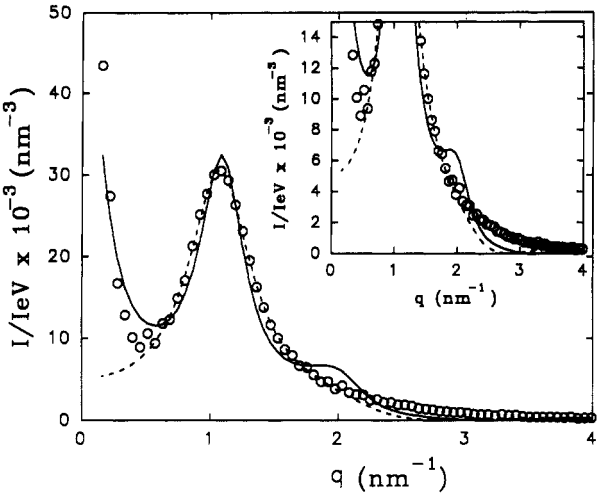

Figure 8. Comparison of adhesive hard sphere model (—) and Yarusso monodisperse hard sphere model (– –) to experimental data (O) for M2SNa.

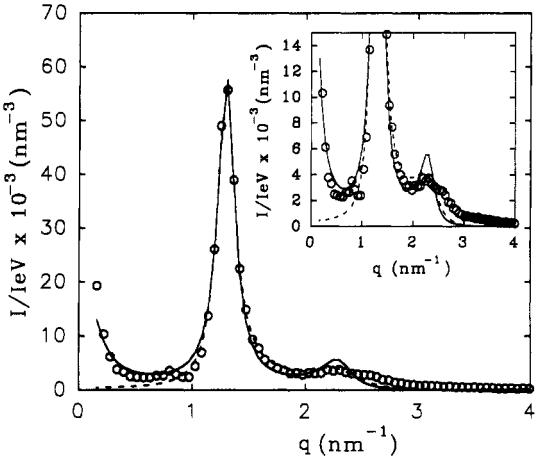

Figure 9. Comparison of adhesive hard sphere model (—) and Yarusso monodisperse hard-sphere model (– –) to experimental data (O) for P2SNa.

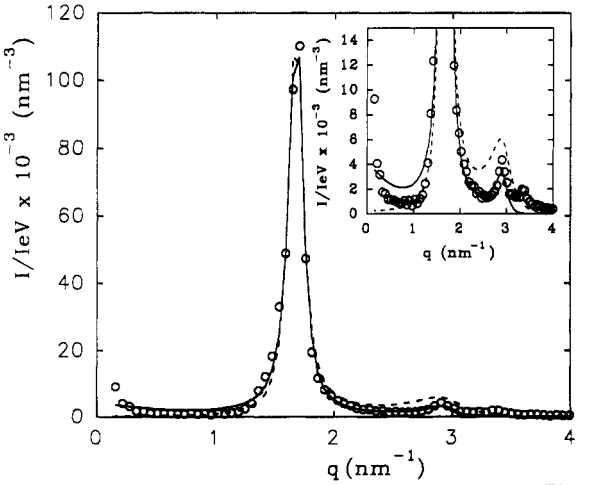

Figure 10. Comparison of adhesive hard sphere model (—) and Yarusso monodisperse hard-sphere model (– –) to experimental data (O) for P1SNa.

Table IV
Model-Fit Parameters for Local Ordering Model

sample	R, nm	D, nm	$\Delta\rho$, nm^{-3}
M1SNa	1.41	5.33	325
M2SNa	1.54	6.53	266
E1SNa	1.06	4.73	287

Examining the model fit parameters in Table III, values of τ were computed from the best-fit η and λ. Baxter[58] gives the location of the critical point as $\tau_c = 0.0976$, $\eta_c = 0.1213$. Thus, the τ values for M1SNa and M2SNa are both supercritical; no physical inconsistency is posed. The τ values for P1SNa and P2SNa are both negative, however, clearly in contravention of the basic assumption of the model. Furthermore, the best-fit $\Delta\rho$ values for M1SNa and M2SNa are large and would require the aggregates be free of both polymer matrix material and any degree of hydration. Both conditions are highly unlikely. Thus, while the qualitative fits of many features of the ionomer SAXS pattern can be achieved with the adhesive hard-sphere model, the physical inconsistency of the model parameters, as well as the number of model parameters, severely limits the usefulness of the model in describing ionomer morphology.

Local Ordering Model. In a recent paper on small-angle neutron scattering (SANS) from hydrated Nafion ionomers, Dreyfus et al.[61] introduced a new model of ionomer morphology to describe their SANS results. The model describes a locally ordered structure for the ionic aggregates. A central aggregate is surrounded by four first neighbors at a distance D. The neighbors are tetrahedrally coordinated to the central aggregate. The diamondlike local structure was postulated because it allows the smallest extension for segments of polymer linking two adjacent aggregates. As such a highly ordered structure cannot extend over long distances in ionomeric materials that are recognized as amorphous, the model further postulates that, at distances greater than αD ($\alpha > 1$), the aggregates are arranged in a completely disordered gaslike state.

The scattering equations that describe the local ordering model, adapted for SAXS analysis of dry ionomers, are

$$\frac{I}{I_e V} = \frac{1}{v_p}\left[\frac{4\pi R^3}{3}\right]^2 (\Delta\rho)^2 \Phi^2(qR) S(q) \tag{26}$$

$$S(q) = 1 + z\frac{\sin(qD)}{qD} - z'\Phi(\alpha q D) \tag{27}$$

where v_p is the average sample volume per particle, R is the radius of the spherical aggregate, $\Delta\rho$ is the electron density difference between the aggregate and the matrix, z is the number of neighbors of the central micelle, and z' is the number of micelles in volume $4\pi(\alpha D)^3/3$ corresponding to the "hole" between 0 and αD in the radial distribution function:

$$z' = \frac{4\pi}{3}\frac{(\alpha D)^3}{v_p} \tag{28}$$

While the local ordering model will permit modeling of local structures other than the diamondlike structure, the initial analyses were completed using the local ordering parameters suggested by Dreyfus et al.:[61] $z = 4.0$, $z' = 4.0$, $\alpha = 1.137$. The best-fit model parameters obtained with this local structure are listed in Table IV, and the model fits are shown in Figures 11–13. While the model qualitatively reproduces the data, the quantitative fit is poor. For M1SNa, the peak intensity predicted by the model is less than that seen in the experimental data, and the model overestimates the q range of the upturn. Had

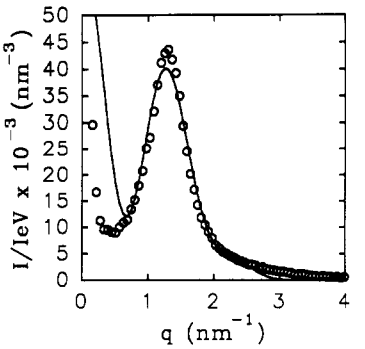

Figure 11. Fit of local ordering model to experimental small-angle X-ray scattering data for M1SNa: model fit (—), experimental data (o).

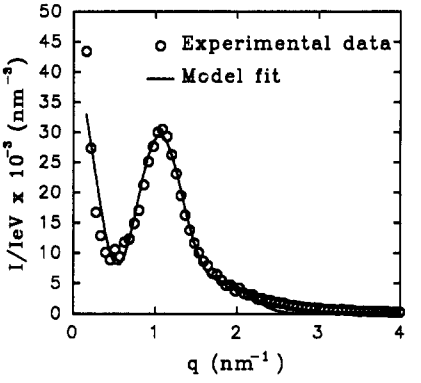

Figure 12. Fit of local ordering model to experimental SAXS data for M2SNa.

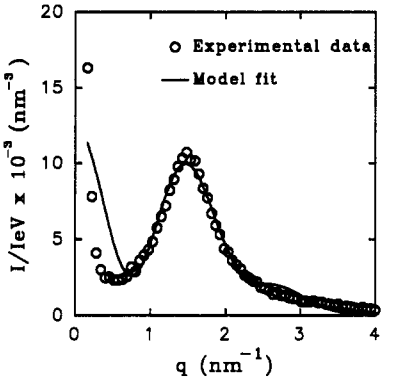

Figure 13. Fit of local ordering model to experimental SAXS data for E1SNa.

the model underestimated the q range of the upturn, the upturn could have been attributed to another source of scattering, such as the inhomogeneous distribution of ionic groups discussed above. An overprediction points to a faulty model. A better fit to the data is seen for M2SNa, but again, the q range of the upturn is slightly overestimated. Finally, for E1SNa, while a peak and an upturn are predicted, the quantative agreement with the data is marginal. Attempts to model the P1SNa and P2SNa data were unsuccessful, as the model was unable to reproduce their narrow ionomer peaks.

Attempts were made to generate better quantitative agreement between model and data by varying z, z', and α. No combination of the six model parameters could be found that gave significantly better fits to the data. Thus, while a local ordering model was highly successful in modeling SANS data from dry and hydrated Nafion ionomers, it does not appear to be applicable in the modeling of SAXS data from other types of dry ionomers.

Conclusions

SAXS analysis of carboxylated and sulfonated model polyurethane ionomers using a liquidlike hard-sphere model reveals that carboxylated ionomers have lower degrees of phase separation, larger aggregate sizes, and lower aggregate number densities than their sulfonated analogues. The effect of polyol type on ionomer morphology was similar for carboxylated and sulfonated ionomers, with average spacings between aggregates being greatest for the PTMO-based ionomers, followed by the PEO-based and finally the PPO-based ionomers. P1SNa exhibited a substantial degree of ordering of the ionic aggregates, in contrast to the other ionomers investigated; the four observable SAXS peaks for P1SNa agreed with spacings expected for spherical particles distributed on either a simple cubic or body-centered cubic lattice. (The scattering patterns for the two lattice types are indistinguishable up to the seventh order scattering peak. As no seventh or higher order scattering peak was visible, the ambiguity in lattice type cannot be resolved with the data presented here.) Polyol molecular weight was shown to have a strong effect on the morphology of carboxylated PPO-based ionomers; ionic aggregation occurred in the P2CNa ionomer but not in the P1CNa ionomer. Increases in ionic aggregate radius and average volume per particle were observed with increasing polyol molecular weight for all the fully substituted ionomers, as expected.

Three models of ionomer morphology, in addition to the liquidlike hard-sphere model, were investigated to determine their utility in analyzing ionomer SAXS data. Both the adhesive hard-sphere model and the local ordering model provided qualitative reproductions of the upturn and the peak in ionomer data. However, neither model provided good quantitative agreement with the data with physically reasonable parameters. In contrast, the liquidlike polydisperse hard-sphere model gave an excellent fit to the ionomer peak and the high-q tail. In the PTMO- and PPO-based ionomers, where polydispersity was expected to be low, little change in model parameters was observed between the original Yarusso model[8] and this model. However, in an ionomer where aggregate size polydispersity was expected to be greater, E1SNa, a substantial difference in morphological parameters was seen. The morphological information derived from the polydisperse hard-sphere model is thus expected to more accurately reflect the morphology of the ionomer. Furthermore, the great improvement in the fit of the high-q data over that given by the original Yarusso model[8] shows that a truly quantitative modeling of ionomer SAXS data requires consideration of polydispersity effects. The liquidlike polydisperse hard-sphere model is proposed as a model that is capable of quantitatively modeling the characteristic SAXS peak and the high-q tail of ionomer scattering data with physically reasonable parameters.

Acknowledgment. Support for this work was provided by U.S. Department of Energy through Grant DE-FG02-88ER45370, by the donors of the Petroleum Research Fund, administered by the American Chemical Society, and by Fellowships for S.A.V. from the National Science Foundation and the Wisconsin Alumni Research Foundation.

References and Notes

(1) Eisenberg, A.; King, M. *Ion Containing Polymers: Physical Properties and Structure*; Academic Press: New York, 1977.
(2) MacKnight, W. J.; Earnest, T. *Macromol. Sci., Rev. Macromol. Chem.* **1981**, *16*, 41.
(3) Eisenberg, A., Bailey, F., Eds. *Coulombic Interactions in Macromolecular Systems*; ACS Symposium Series No. 302; American Chemical Society: Washington, D.C., 1986.
(4) Tant, M.; Wilkes, G. *J. Macromol. Sci., Rev.* **1988**, *C28*, 1.
(5) Lantman, C. W.; MacKnight, W. J.; Lundberg, R. D. *Annu. Rev. Mater. Sci.* **1989**, *19*, 295.
(6) Fitzgerald, J. J.; Weiss, R. A. *J. Macromol. Sci., Rev.* **1988**, *C28*, 99.
(7) Pineri, M., Eisenberg, A., Eds. *Structure and Properties of Ionomers*; NATO ASI Series *198*; D. Reidel Publishing Co.: Dordrecht, Holland, 1987.
(8) Yarusso, D. J.; Cooper, S. L. *Macromolecules* **1983**, *16*, 1871.
(9) Eisenberg, A. *Macromolecules* **1970**, *3*, 147.
(10) Toriumi, H.; Weiss, R. A.; Frank, H. A. *Macromolecules* **1984**, *17*, 2104.
(11) Takei, M.; Tsujita, Y.; Shimada, S.; Ichihara, H.; Enokida, M.; Takizawa, A.; Kinoshito, T. *J. Polym. Sci.: Polym. Phys. Ed.* **1988**, *26*, 997.
(12) Brozoski, A.; Coleman, M. M.; Painter, P. C. *J. Polym. Sci.: Polym. Phys. Ed.* **1983**, *21*, 301.
(13) Eisenberg, A.; Hird, B.; Moore, R. B. *Macromolecules* **1990**, *23*, 4098.
(14) Register, R. A.; Pruckmayr, G.; Cooper, S. L. *Macromolecules* **1990**, *23*, 3023.
(15) Register, R. A.; Cooper, S. L.; Thiyagarajan, P.; Chakrapani, S.; Jerome, R. *Macromolecules* **1990**, *23*, 2978.
(16) Hashimoto, T.; Fujimura, M.; Kawai, H. In *Perfluorinated Ionomer Membranes*; Eisenberg, A., Yeager, H. L., Eds.; ACS Symposium Series No. 180; American Chemical Society: Washington, D.C., 1982; p 217.
(17) Fujimara, M.; Hashimoto, T.; Kawai, H. *Macromolecules* **1982**, *15*, 136.
(18) Roche, E. J.; Stein, R. S.; Russell, T. P.; MacKnight, W. J. *J. Polym. Sci.: Polym. Phys. Ed.* **1980**, *18*, 1497.
(19) MacKnight, W. J.; Taggart, W. P.; Stein, R. S. *J. Polym. Sci., Polym. Symp.* **1974**, *45*, 113.
(20) Lee, D. C.; Register, R. A.; Yang, C. Z.; Cooper, S. L. *Macromolecules* **1988**, *21*, 998.
(21) Marx, C. L.; Caulfield, D. F.; Cooper, S. L. *Macromolecules* **1973**, *6*, 344.
(22) Williams, C. E.; Russell, T. P.; Jerome, R.; Horrion, J. *Macromolecules* **1986**, *19*, 2877.
(23) Kinning, D. J.; Thomas, E. L. *Macromolecules* **1984**, *17*, 1712.
(24) Kinning, D. J.; Thomas, E. L.; Fetters, L. J. *J. Chem. Phys.* **1989**, *90*, 5806.
(25) Register, R. A.; Pruckmayr, G.; Cooper, S. L. *Macromolecules* **1990**, *23*, 3023.
(26) Yarusso, D. J.; Cooper, S. L. *Polymer* **1985**, *26*, 371.
(27) Ding, Y. S.; Register, R. A.; Yang, C.-Z.; Cooper, S. L. *Polymer* **1989**, *30*, 1213.
(28) Visser, S. A.; Cooper, S. L. *Macromolecules*, previous paper in this issue.
(29) Lake, J. A. *Acta Crystallogr.* **1967**, *23*, 191.
(30) Kratky, O.; Pilz, I.; Schmitz, P. J. *J. Colloid Interface Sci.* **1966**, *21*, *24*.
(31) Porod, G. *Kolloid Z.* **1951**, *124*, 83.
(32) Koberstein, J. T.; Stein, R. S. *J. Polym. Sci.: Polym. Phys. Ed.* **1983**, *21*, 1439.
(33) Kao, J.; Stein, R. S.; MacKnight, W. J.; Taggart, W. P.; Cargill III, G. *Macromolecules* **1974**, *7*, 95.
(34) Fujimara, M.; Hashimoto, T.; Kawai, H. *Macromolecules* **1981**, *14*, 1309.
(35) Fujimara, M.; Hashimoto, T.; Kawai, H. *Macromolecules* **1982**, *15*, 136.
(36) Geirke, T. D.; Munn, G. E.; Wilson, F. C. *J. Polym. Sci.: Polym. Phys. Ed.* **1981**, *24*, 1687.
(37) Fournet, G. *Acta Crystallogr.* **1951**, *4*, 293.
(38) Kinning, D. J.; Thomas, E. L. *Macromolecules* **1984**, *17*, 1712.
(39) Percus, J. K.; Yevick, G. *Phys. Rev.* **1958**, *110*, 1.
(40) Wertheim, M. S. *Phys. Rev. Lett.* **1963**, *10*, 321.
(41) Thiele, E. *J. Chem. Phys.* **1963**, *39*, 474.
(42) Barker, J. A.; Henderson, D. *Rev. Mod. Phys.* **1976**, *48*, 587.
(43) Kramendank, W. G. T.; Frenkel, D. *Mol. Phys.* **1988**, *64*, 403.
(44) Lord Rayleigh, *Proc. R. Soc. London* **1914**, *A90*, 219.
(45) Ding, Y. S.; Hubbard, S. R.; Hodgson, K. O.; Register, R. A.; Cooper, S. L. *Macromolecules* **1988**, *21*, 1698.
(46) Miller, R. L. In *Polymer Handbook*, 3rd ed.; Brandrup, J., Immergut, E. H., Eds.; John Wiley and Sons: New York, 1989; p IV-72.

(47) Arco Chemical, Thanol PPG-2000, Polyol Product Data, 1988.
(48) Van Bogart, J. W. C. Ph.D. Thesis, University of Wisconsin, 1981; p 225.
(49) Broze, G.; Jerome, R.; Teyssie, Ph. *J. Polym. Sci.: Polym. Lett. Ed.* **1981**, *19*, 415.
(50) Ledent, J.; Fontain, F.; Reynaers, H.; Jerome, R. *Polym. Bull.* **1985**, *14*, 461.
(51) Feng, D.; Wilkes, G. L.; Leir, C. M.; Stark, J. E. *J. Macromol. Sci. Chem.* **1989**, *A26*, 1151.
(52) DePorter, C. D.; Venkateschwaran, L. N.; York, G. A.; Wilkes, G. L.; McGrath, J. E. *Polym. Prepr. (Am. Chem. Soc., Div. Polym. Chem.)* **1989**, *30*, 201.
(53) Li, C.; Register, R. A.; Cooper, S. L. *Polymer* **1989**, *30*, 1227.
(54) Vrij, A. *J. Chem. Phys.* **1979**, *71*, 3267.
(55) Register, R. A. Ph.D. Thesis, University of Wisconsin, 1989; p 305.
(56) Wu, D. Q.; Phillips, J. C.; Lundberg, R. D.; MacKnight, W. J.; Chu, B. *Macromolecules* **1989**, *22*, 992.
(57) Tant, M. R.; Wilkes, G. L. *J. Appl. Polym. Sci.* **1989**, *37*, 2873.
(58) Baxter, R. J. *J. Chem. Phys.* **1968**, *49*, 2770.
(59) Regnaut, C.; Ravey, J. C. *J. Chem. Phys.* **1989**, *91*, 1211.
(60) Regnaut, C.; Ravey, J. C. *J. Chem. Phys.* **1990**, *92*, 3250.
(61) Dreyfus, B.; Gebel, G.; Aldebert, P.; Pineri, M.; Escoubes, M.; Thomas, M. *J. Phys. (France)* **1990**, *51*, 1341.